Published online 13 January 2010

Nucleic Acids Research, 2010, Vol. 38, No. 9 ***2851–2864***
doi:10.1093/nar/gkp1236

DnaB proteolysis *in vivo* regulates oligomerization and its localization at *oriC* in *Bacillus subtilis*

William H. Grainger[1], Cristina Machón[1], David J. Scott[2] and Panos Soultanas[1,*]

[1]Centre for Biomolecular Sciences, University of Nottingham, University Park, Nottingham NG7 2RD and [2]The National Centre for Molecular Hydrodynamics, School of Biosciences, Sutton Bonington Campus, Leicestershire LE12 5RD, UK

Received October 20, 2009; Revised December 23, 2009; Accepted December 24, 2009

ABSTRACT

Initiation of bacterial DNA replication at *oriC* is mediated by primosomal proteins that act cooperatively to melt an AT-rich region where the replicative helicase is loaded prior to the assembly of the replication fork. In *Bacillus subtilis*, the *dnaD*, *dnaB* and *dnaI* genes are essential for initiation of DNA replication. We established that their mRNAs are maintained in fast growing asynchronous cultures. DnaB is truncated at its C-terminus in a growth phase-dependent manner. Proteolysis is confined to cytosolic, not to membrane-associated DnaB, and affects oligomerization. Truncated DnaB is depleted at the *oriC* relative to the native protein. We propose that DNA-induced oligomerization is essential for its action at *oriC* and proteolysis regulates its localization at *oriC*. We show that DnaB has two separate ssDNA-binding sites one located within residues 1–300 and another between residues 365–428, and a dsDNA-binding site within residues 365–428. Tetramerization of DnaB is mediated within residues 1–300, and DNA-dependent oligomerization within residues 365–428. Finally, we show that association of DnaB with the *oriC* is asymmetric and extensive. It encompasses an area from the middle of *dnaA* to the end of *yaaA* that includes the AT-rich region melted during the initiation stage of DNA replication.

INTRODUCTION

Bacterial DNA replication initiates at *oriC* with the recruitment of two replicative helicases and associated primases around which two replisomes assemble to start copying the parental genome. The replication initiator protein DnaA is ubiquitous but replication initiation mechanisms and their regulatory processes vary between bacteria (1), probably reflecting the different architectures of their replication origins (2,3). DnaA binds to specific sites within *oriC* to assist local melting in an AT-rich region for loading of the replicative helicase (4–6). During the elongation phase of DNA replication, replication forks are frequently challenged by mutations, nicks, base modifications and other factors, resulting in fork arrest and collapse. Recombination-based and direct repair mechanisms re-initiate replication from stalled sites (7). In *Escherichia coli* two restart mechanisms, PriA- and PriC-mediated, differ in their ability to recognize nascent DNA at stalled forks (8). PriA, like DnaA, is ubiquitous but other primosomal proteins are not. For example, *Bacillus subtilis* does not have homologues of *E. coli* PriB, PriC and DnaT. Instead, two *B. subtilis* proteins DnaB and DnaD are required for initiation of DNA replication at *oriC* and stalled replication fork sites (9–12). No homologues of these proteins are found in gram negative bacteria implying that their replication initiation mechanisms are different.

Mechanistic and regulatory details of *B. subtilis* replication initiation are not clear at present. DnaD interacts with DnaA (13) and PriA (14) and is likely to act in the early stages of primosomal assembly while DnaB acts at a later stage. In fact DnaB is believed to be recruited to the *oriC*–DnaA–DnaD complex by an interaction with DnaD. DnaD has DNA remodelling activity on supercoiled DNA (15–17) and counteracts the lateral DNA compaction activity of DnaB (18). The DNA remodelling activity of DnaD is the sum of oligomerization and DNA-binding activities on two separate domains. An N-terminal domain mediates scaffold formation (19,20) and a C-terminal domain binds to DNA and has a second DNA-induced oligomerization interface (19). DnaB is multifunctional; it interacts with DnaD on SSB-coated DNA (21), cooperates with DnaI (the helicase loader homologous to *E. coli* DnaC) as 'co-loader' of DnaC (the replicative helicase homologous to *E. coli* DnaB)

*To whom correspondence should be addressed. Tel: +44 115 9513525; Fax: +44 115 8468002; Email: panos.soultanas@nottingham.ac.uk

The authors wish it to be known that, in their opinion, the first two authors should be regarded as joint First Authors.

(22,23), acts as an origin membrane attachment protein (24–28), regulates the recruitment of DnaD to the membrane attached *oriC* (29), laterally condenses supercoiled DNA (18) and is essential for regulation of replication initiation synchrony (12).

We found that DnaB is truncated *in vivo* to smaller polypeptides in middle to late exponential growth and late stationary phases. This truncation takes place in a C-terminal domain, which is responsible for DNA-induced higher-order oligomerization, and is confined to cytosolic, not membrane-associated, DnaB. Using truncated polypeptides we found that DnaB(1–428) forms nucleoprotein complexes similar to those formed by native DnaB, whereas DnaB(1–365) is defective in DNA-induced oligomerization. Tetrameric $DnaB_N$ (residues 1–300) binds to ssDNA, not dsDNA, and does not form high-order complexes, while a monomeric $DnaB_C$ (residues 301–472) binds to ss and dsDNA and forms higher-order nucleoprotein complexes. Therefore, the dsDNA-binding site of DnaB is located within residues 365–428. Tetramerization of DnaB is mediated within residues 1–300 and DNA-dependent oligomerization within residues 365–428.

ChIP-chip analysis revealed that, relative to full-length DnaB, truncated DnaB is depleted at *oriC*. There is no significant difference in the mRNA levels of the *dnaB, dnaD* and *dnaI* primosomal genes during exponential growth of asynchronous cultures. We propose that DnaB functional regulation in asynchronous cultures is posttranslational and involves proteolytic truncation of its C-terminal domain. Proteolysis of DnaB abolishes high-order DNA-induced oligomerization and regulates its localization at *oriC*. Truncated DnaB in the stationary phase may bind DNA but will not form higher-order oligomers, and may be essential for functions other than initiation of DNA replication.

MATERIALS AND METHODS

RNA purification and cDNA synthesis

B. subtilis strain 168 was cultured in Luria–Bertani (LB) media. An overnight culture was diluted into LB and incubated at 30 °C. Samples were harvested at $OD_{600} = 0.3$ (lag phase, t_1), 0.9 (exponential phase, t_2), 1.3 (early stationary phase, t_3) and overnight (late stationary phase, t_4) for RNA and protein isolation. RNA was extracted from 4 ml cell cultures using RNAprotect Bacteria Reagent and Qiagen RNeasy Mini Columns (Qiagen), according to manufacturer's instructions, except for a 10 s sonication step after the addition of lysozyme and Proteinase K. DNaseI digestion was performed, as described in the Qiagen protocol. RNA was quantified by a NanoDrop ND-1000 (Thermo Scientific), its quality checked by capillary electrophoresis in an Agilent 2100 Bioanalyzer (Agilent Technologies) and stored at −20 °C. cDNA synthesis was carried out with random primers and SuperScript II Reverse Transcriptase (Invitrogen) according to the manufacturer's instructions.

RT–PCR. Primers were designed with Primer Express 3.0 software (PE Applied Biosystems) (Supplementary Figure 1S). RT–PCR reactions were carried out using PowerSYBR green Master Mix on a 7500 Real-Time PCR system (PE Applied Biosystems). Equal amounts of cDNA (5 ng) and 300 nM primers were used in all amplification reactions. PCR conditions were: one cycle of 50°C for 2 min, one cycle of 95°C for 10 min, 40 cycles of 95°C for 15 s and 60°C for 15 s and one cycle of 60°C for 1 min. Product formation was monitored by fluorescence increase from SYBR Green intercalation. The threshold cycle (C_T) is the first cycle for which a statistically significance increase in the amount of product is detected. C_T values are thus inversely proportional to the cDNA amount in the sample. Relative quantification was used as described before (30) to determine changes in *dnaB*, *dnaD* and *dnaI* expression compared to *sigA* (ΔC_T value), followed by comparisons of the three genes over time ($\Delta\Delta C_T$ value). Relative quantification was done using the formula $2^{-\Delta\Delta c_T}$ as described previously (30).

Protein extraction and western-blot analysis

Cell pellets from 10 ml cultures were suspended in 1 ml 50 mM Tris–HCl pH 7.5, 500 mM NaCl, 1 mM EDTA and sonicated 3 × 10 s. The soluble fraction was separated by centrifugation at 13 000 rpm for 5 min at room temperature. The membrane fraction (pellet) was washed twice with the same buffer before suspension in 8 M urea. Protein was quantified by Bradford assay (31). Extracts were resolved by SDS–PAGE and transferred to nitrocellulose membranes (Hybond-ECL, GE Healthcare) by electrotransfer in Tris–Glycine buffer (12.5 mM Tris pH 9.0, 96 mM glycine and 20% v/v methanol). Membranes were blocked overnight with 10% w/v dried milk in PBS-T (20 mM phosphate buffer, pH 7.2, 150 mM NaCl, 0.05% v/v Tween-20) and washed 3 × 5 min with PBS-T before incubation with relevant antibodies for 60–90 min. After washing with PBS-T for 3 × 5 min membranes were incubated with secondary anti-rabbit IgG HandL Chain Specific Peroxidase Conjugate (Calbiochem) and washed with PBS for 5 min. Detection was performed either by SuperSignal® West Pico Chemiluminescence Substrate (Pierce) using Hyperfilm™ ECL films (GE Healthcare) or by the peroxide/DAB method (32). Duplicate gels were run concurrently with the same samples for Coomassie Blue staining. Polyclonal rabbit antibodies were produced by the Medical and Health Sciences support unit at the University of Nottingham and their efficiency was tested by western blots with purified proteins (data not shown). The C-terminal DnaB peptide DLEEQKKKMMEEM QKLKKYSAY was synthesized by Alta Bioscience (Birmingham) and sheep polyclonal antibody against it was made by the Scottish National Blood Transfusion Service. The antibody was purified further by Alta Bioscience using affinity chromatography with a column containing immobilized peptide and supplied in lyophilized 1 mg aliquots. Binding to native DnaB and $DnaB_C$ and failure to bind to $DnaB_N$ were verified by western blotting (Supplementary Figure 2S).

Protein expression and purification

Native untagged DnaB was expressed from pET28a-dnaB and purified as described before (18). Plasmid constructs for N-terminally His_6-DnaB polypeptides were prepared by PCR (Supplementary Figure 1S) using pET28a-dnaB (18) and subcloning into the NdeI/BamHI sites of pET28a (Novagen). DnaD and DnaI were purified as before (33, 15). DnaB polypeptides were expressed at 20°C for 20 h [DnaB and DnaB(1–300)] or 65 h [DnaB(1–356) and DnaB(1–428)] in *E. coli* BL21(DE3) with 1 mM isopropyl-β-D-thiogalactopyranoside (IPTG). Cell pellets were suspended in 20 ml of 50 mM sodium phosphate pH 7.4, 500 mM NaCl, 20 mM imidazole, 1 mM DTT, 10% w/v sucrose, 1 mM phenylmethyl sulfonate and protease inhibitor cocktail (P8849, Sigma; 100 µl/l of culture). Following sonication and clarification by centrifugation (42 000*g* × 40 min at 4°C) the supernatant was filtered (0.2 µm filter, Sartorius) and loaded onto a Ni^{2+}-charged 5 ml HiTrap chelating column (GE Healthcare) equilibrated in buffer A (50 mM sodium phosphate pH 7.4, 500 mM NaCl, 20 mM imidazole, 1 mM DTT). The column was washed successively with 40 ml of buffer A with 2 M NaCl, buffer A with 1% v/v Triton X-100, dH_2O and finally buffer A. Proteins were eluted with a 20–500 mM imidazole gradient over 60 ml. Relevant fractions were pooled and thrombin added (Novagen) at 0.4 units/mg of His_6-DnaB(301–472) or half that for other proteins. After digestion for 16 h at 20°C proteins were buffer-exchanged into buffer A and loaded onto the chelating column equilibrated in buffer A. The flow-through was spin-concentrated and loaded onto a Superdex 200 HiLoad 26/60 column (GE Healthcare), or, in the case of DnaB(301–472), a Superdex 75, equilibrated in buffer C (50 mM Tris–HCl, pH 7.5, 1 mM EDTA, 1 mM DTT, 100 mM NaCl). Relevant fractions were pooled glycerol added to 10% v/v, proteins quantified with a NanoDrop and stored at −80°C.

Analytical ultracentrifugation

Sedimentation velocity was carried out at 40 000 rpm at 20°C, in a Beckman XL-A. Cells were scanned at 280 nm every 5 min. Samples were loaded into two SEDVEL60K channels (SpinAnalytical, NH, USA). Data were analysed using the maximum entropy, c(s), method of Schuck (34) using the program SEDFIT (34–36). Sedimentation equilibrium was attained at 12 000, 16 000 and 20 000 rpm. Data were processed and fitted using SEDFIT and SEDPHAT (http://www.analyticalultracentrifugation.com).

Gel shifts

Oligonucleotides used in gel shift experiments were gel-purified. Radiolabelling was carried out with [γ^{32}P]ATP (Perkin-Elmer) and T4 polynucleotide kinase (NEB). Probes were further purified in 10 mM Tris–HCl pH 8.0 using Sephacryl S-200 columns (GE healthcare). Annealing conditions for the ds dTA_{135} probe were determined carefully before preparation of the final substrate. DnaB and its polypeptides were incubated for 20 min at 25°C with 0.46 nM DNA substrates (dT_{45}, dT_{90}, dT_{135} or dAT_{135}) in 82 mM Tris–HCl pH 7.5, 1.64 mM EDTA, 1.64 mM DTT, 5 mM $MgCl_2$, 100 mM NaCl and 8% v/v glycerol. Samples were resolved by electrophoresis through a chilled (4°C) 18 × 16 cm gel in 0.5 × TBE for 200 min at 200 V. Gels were dried and visualized using a Personal Molecular Imager FX with Quantity-One software (Bio-Rad).

Peptide mass fingerprinting and N-terminal sequencing

Matrix assisted laser desorption ionization-peptide mass fingerprinting (MALDI-PMF) analysis was carried out at the Biopolymer Synthesis and Analysis unit at the University of Nottingham. Following in-gel trypsinization DnaB fragments were excised and eluted from the gel, and peptide spectra were obtained by MALDI. Peptides were identified by Mascot analysis (http://www.matrixscience.com) from databases containing Eubacteria sequences. N-terminal sequencing of intact DnaB fragments excised from gels was carried out by Alta Bioscience (University of Birmingham).

ChIP-chip microarray analysis

Sample preparation for ChIP-chip analysis was carried out as described before (37) with minor modifications. An overnight culture of *Bacillus subtilis* (strain 168) was diluted into 800 ml LB and incubated at 30°C. At mid-log phase (OD_{595} = 0.8) 1% v/v formaldehyde was added for 20 min to cross-link protein–DNA complexes and the reaction was quenched by 0.5 M glycine. Cells were harvested and washed with 50 ml 10 mM Tris–HCl pH 7.5, suspended in 2 ml lysis buffer (10 mM Tris–HCl pH 8.0, 20% w/v sucrose, 50 mM NaCl, 10 mM EDTA, 10 mg/ml lysozyme) and incubated at 37°C for 30 min. Immunoprecipitation (IP) buffer (8 ml) was added (50 mM HEPES–KOH pH 7.5, 150 mM NaCl, 1 mM EDTA, 1% v/v Triton X-100, 0.1% w/v sodium deoxycholate, 0.1% w/v sodium dodecyl sulfate and 1 mM phenylmethylsulfonyl fluoride) and the solution sonicated 15 times (20 s bursts, 20 s rest on ice). The mixture was clarified by centrifugation (15 000*g*, 15 min at 4°C), the supernatant incubated with 300 µl anti-DnaB antibody overnight at 4°C on a rotating wheel and then with 150 µl of Dynabeads® M-280 sheep anti-rabbit IgG (Invitrogen) for 5 h at 4°C. The beads were washed twice with IP buffer, once with wash buffer (10 mM Tris–HCl pH 8.0, 250 mM LiCl, 1 mM EDTA, 0.5% v/v Nonident-P40 and 0.5% w/v sodium deoxycholate), once with wash buffer plus 0.02 M NaCl and twice with TE buffer (10 mM Tris–HCl pH 7.5, 1 mM EDTA). After removing the TE buffer, the beads were suspended in 400 µl elution buffer (50 mM Tris–HCl pH 7.5, 10 mM EDTA, 1% w/v SDS) and incubated at 65°C for 10 min. Cross links were reversed by incubation with 0.8 mg/ml of proteinase K (Thermo Scientific) in 0.5× elution buffer at 42°C for 2 h and 65°C for 6 h. DNA was purified with a PCR purification kit (QIAGEN) and quantified by Nanodrop.

B. subtilis (strain 168) Agilent 4x44K ChIP arrays with AMADID 023001 were prepared by Oxford Gene Technologies (OGT) who carried out array hybridization analysis and provided the final data. Each array comprises 41 770 probes in total, covering 4 185 genes. Each probe is 60 bp and generated using Agilent's inkjet *in-situ* synthesis technology. The probes have an average spacing of ~100 bp with a maximum inter-probe distance of ~140 bp. The reference sample in the red (Cy5) channel was genomic *B. subtilis* (strain 168) DNA. Data analysis was carried out with a ChIP browser developed and supplied by OGT.

RESULTS

The mRNAs of the *dnaD*, *dnaB* and *dnaI* genes are maintained throughout asynchronous growth

Regulation of initiation of DNA replication is linked to the balance between DnaA levels and the number of DnaA-binding sites in the cell (38, 39). DnaA is regulated at the transcriptional level (39). The fate of the mRNAs of other primosomal genes during growth is unknown. We investigated the mRNA levels of *dnaD*, *dnaB* and *dnaI* during growth of asynchronous *B. subtilis* cultures by quantitative RT-PCR. Control experiments to verify direct proportionality between amounts of RNA and PCR signals were carried out and data were normalized against the *sigA* mRNA (data not shown). *SigA* codes for σ^A which is essential for transcription of housekeeping genes. Its mRNA remains constant during exponential growth (40). Comparison of C_T values from RT-PCR experiments revealed that mRNA levels of *dnaB*, *dnaI* and *dnaD* were constant throughout growth (Figure 1A). The *dnaB* and *dnaI* genes are juxtaposed in the same operon (41) while *dnaD* is located in a distant operon. C_T values indicated that the mRNA levels of *dnaB* and *dnaI* were identical and *dnaD* slightly higher (Figure 1A). Normalization against *sigA* mRNA and direct comparisons of ΔC_T values indicated similar levels for each of the three mRNAs at t_1 (early growth-phase) and t_2 (middle growth phase) and only a marginal decrease at t_3 (late growth phase) that was statistically insignificant. It was not possible to normalize samples from late stationary growth phase relative to each other as control *sigA* mRNA levels were not constant in these samples (data not shown). Attempts to use a different control, 16S rRNA, were unsuccessful because of growth dependent variability (data not shown). From these data we conclude that the mRNAs of *dnaD*, *dnaB* and *dnaI* are maintained throughout asynchronous growth.

C-terminal proteolytic truncation of DnaB in a growth phase dependent manner

Western blots of *B. subtilis* extracts from overnight cultures, using polyclonal rabbit antibodies against DnaB, DnaD and DnaI, confirmed the presence of all three proteins (Figure 1B). However, DnaB polypeptides noticeably smaller than the native size (MW 55 171 Da) were apparent (Figure 1B). Truncation of DnaB *in vivo* was postulated before but no experimental evidence has

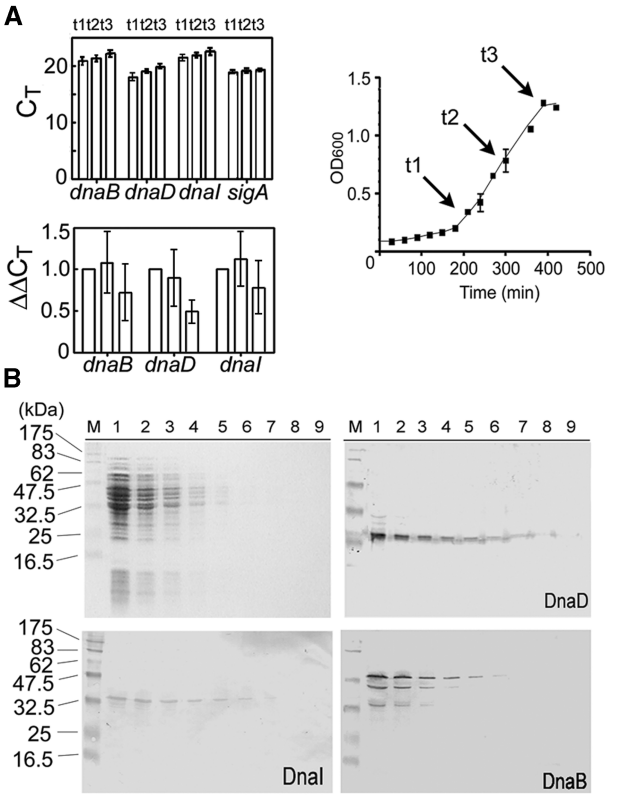

Figure 1. Growth-dependent expression of *dnaD*, *dnaI* and *dnaB* genes. (**A**) Growth curve of *B. subtilis* strain 168 in LB at 30°C over time. Time points t_1, t_2 and t_3 when samples were analysed are indicated. The top bar graph shows levels of *dnaB*, *dnaD*, *dnaI* and *sigA* as C_T values from RT-PCR over time. The bottom bar graph shows changes in gene expression calculated from the formula $2^{-\Delta\Delta Ct}$ for *dnaB*, *dnaD* and *dna*I, using *sigA* as control and t_1 as calibrator, over time. In both graphs each bar represents the mean of five independent experiments. The error bars indicate standard deviations. (**B**) Western blot analysis of *B. subtilis* soluble extracts from overnight cultures. A typical SDS–PAGE gel with decreasing amounts of extracts (72, 36, 18, 9, 4.5, 2.2, 1.1, 0.5 and 0.25 μg) is shown (top left), with western blots for DnaD, DnaI and DnaB, as indicated. DnaB is truncated to smaller versions. Pre-stained molecular weight markers from New England Biolabs are indicated in kDa.

been published (26). Its nature and biological significance remain a mystery. Heterologous expression of DnaB in *E. coli* and subsequent purification revealed additional smaller polypeptides (Figure 2A and Supplementary Figure 3S). N-terminal sequencing established that they all had the native DnaB N-terminal sequence (data not shown). Random degradation or cleavage of specific domains would be expected to produce peptides of variable N-termini. However, this was not the case. Western blot analysis of cell lysates from *E. coli* expressing DnaB showed that the observed truncation is due to '*in vivo* cleavage' during expression and not due to proteolysis during purification (Figure 2A). Consistent with this, western blot analysis of *B. subtilis* soluble extracts from early and late exponential growth detected native DnaB (~55 kDa) in early growth, and native plus truncated (~40 kDa) DnaB in late growth (Figure 2B). In samples from overnight cultures, a significant fraction of DnaB was truncated suggesting that proteolysis continues

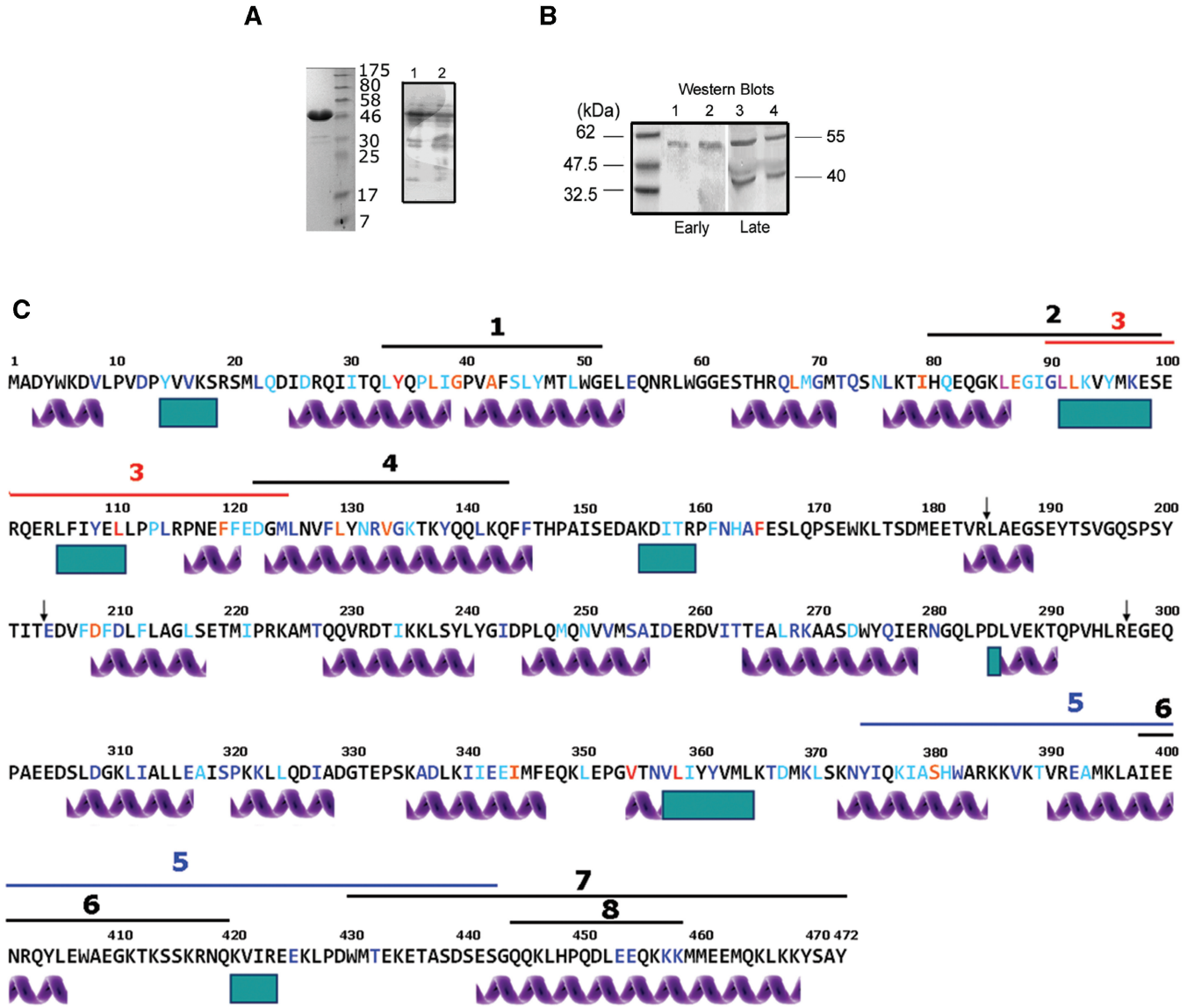

Figure 2. Proteolytic truncation of DnaB. (**A**) Left, SDS–PAGE analysis of DnaB with smaller fragments visible. Truncated fragments are clearly visible in the juxtaposed western blot. Cell extracts from DnaB-expressing *E. coli* were analysed by western blotting (lane 1, whole cell extract; lane 2, soluble fraction). DnaB fragments were present indicating that truncation was occurring during expression and not during purification. (**B**) DnaB western blots of *B. subtilis* soluble extracts from early (lane 1, 20 μg; lane 2, 25 μg) and late (lane 3, 25 μg; lane 4, 20 μg) exponential growth phases, as indicated. DnaB is intact in early growth but a truncated polypeptide (~40 kDa) appears in late growth. (**C**) The primary sequence of *B. subtilis* DnaB (residues 1–472). Predicted α-helices and β-strands (green boxes) are indicated. Secondary-structure prediction was carried out by Jpred 3 (42) and was consistent with several other programs. DnaB residues are colored according to sequence conservation obtained by multiple sequence alignment using Clustal W2 (43) of DnaB proteins from 47 sequenced genomes across the Firmicutes phylum (data not shown); pink (100% identity); red [100% close similarity, score ≥ 2 in the Blosum62 substitution matrix (44)]; orange (100% similarity, Blosum62 score ≥ 0); sky blue (≥90% similarity); dark blue (≥80% similarity). Regions of particular interest are indicated by horizontal lines and are (1) hydrophobic motif (25); (2) putative DNA binding motif (45); (3) 45.7% identity with RTP (46); (4) putative ATP binding motif (25); (5) similarity to Gp49 a putative phage replication initiation protein (29); (6) putative ATP-binding motif (25); (7) trypsin sensitivity (23); and (8) an antibody against a 15 amino acid peptide from this region inhibits binding to the pUB110 plasmid (47). Arrows show cleavage sites in limited proteolysis experiments (23).

into the late stationary growth phase (Figures 1B and 2B). The sizes of fragments did not indicate the appearance of distinct domains that added up to the size of the full-length protein. Instead, the sizes of the fragments were consistent with truncation at its C-terminus and complete digestion of the removed C-terminal fragment.

MALDI-PMF of truncated DnaB polypeptides purified from *E. coli* revealed peptides covering residues 1–411 (Supplementary Figure 3S). The smaller polypeptides, labelled 2–5, produced peptides covering residues 1–289 suggesting that proteolysis takes place at the C-terminus (Supplementary Figure 3S). Previous studies identified two domains at each end (residues 1–184 and 297–472) with a small central domain (residues 204–296), (23). Interestingly, the same studies reported proteolytic sensitivity of the C-terminal region, residues 430–472.

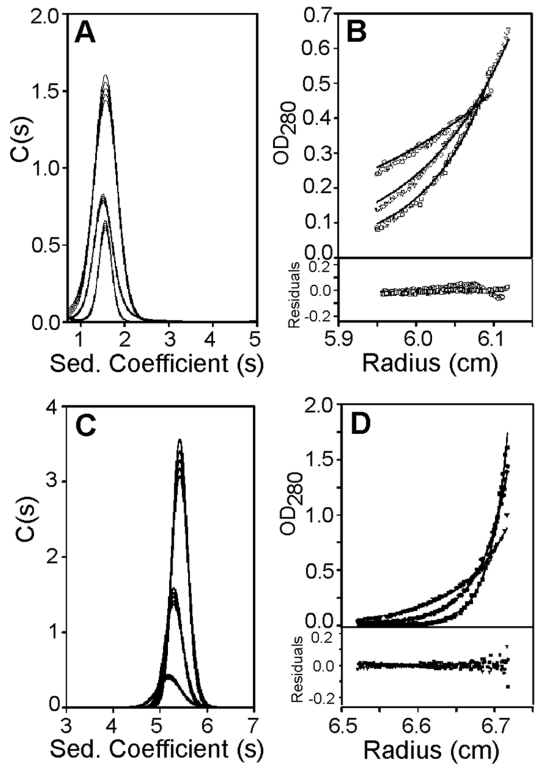

Figure 3. The oligomeric states of the DnaB domains. Sedimentation velocity AUC data for $DnaB_C$ (**A** velocity sedimentation at 40 000 rpm, **B**: equilibrium sedimentation at 17 000, 24 000 and 29 000 rpm) and $DnaB_N$ (**C**: velocity sedimentation at 40 000 rpm, **D**: equilibrium sedimentation at 12 000, 16 000 and 20 000 rpm) reveal that $DnaB_C$ is a monomer, while $DnaB_N$ is tetrameric at higher concentrations but in a dimer–tetramer equilibrium at lower concentrations (K_d = 500 nM). Experiments were carried out at 12.96, 11.25 and 8.07 μM $DnaB_C$ and 21.3, 15.6 and 7.8 μM $DnaB_N$.

We constructed two domains of DnaB encompassing residues 1–300 ($DnaB_N$; N-terminal domain plus the central domain, MW 35 157 Da) and 301–472 ($DnaB_C$; C-terminal domain, MW 20 445 Da), (Figure 2C). $DnaB_C$ was found to be monomeric by analytical ultracentrifugation (Figure 3A and B) whilst $DnaB_N$ was a tetramer at high concentrations and in a dimer-tetramer equilibrium at low concentrations (K_d = 500 nM) (Figure 3C and D). To unequivocally show that the C-terminal region of DnaB was being truncated we raised a sheep polyclonal antibody against a peptide encompassing the last twenty two C-terminal residues (DLEEQKKKMMEEMQKLKKYSAY). We argued that if proteolysis takes place at the C-terminus this antibody will recognize native DnaB but not truncated polypeptides. The antibody was significantly weaker than rabbit anti-DnaB and was not sensitive enough to detect DnaB in *B. subtilis* extracts (data not shown), but it recognized purified native DnaB, $DnaB_C$ and not $DnaB_N$ (Supplementary Figure 2S). It was only useful in establishing that over-expressed DnaB in *E. coli* was truncated from its C-terminus. The combined data show that DnaB is proteolytically truncated *in vivo* from its C-terminus in a growth-dependent manner and analogous truncation is observed when DnaB is heterologously expressed *in E. coli*. It is not clear whether *E. coli* uses the same or different proteases to process DnaB. However, proteolysis of DnaB in *E. coli* is less efficient probably because of its large over-expression in a short period of time.

DnaB has two separate ssDNA binding sites, one in $DnaB_N$ and another in $DnaB_C$, and a ssDNA-dependent oligomerization activity in $DnaB_C$

$DnaB_N$ and $DnaB_C$ did not interact with each other (data not shown) but both bound ssDNA. $DnaB_N$ formed defined complexes with oligonucleotides dT_{45}, dT_{90} and dT_{135}, (Figure 4). The patterns of shifted bands with increasing oligonucleotide sizes suggest that a small fraction of $DnaB_N$ binds as a dimer forming a minor band shifted the least with all three substrates, while most $DnaB_N$ binds as a tetramer to form one major shifted band with dT_{45}, two with dT_{90} (two bound tetramers) and three with dT_{135} (three bound tetramers). Therefore, the apparent $DnaB_N$ footprints are ~45 and 22 nucleotides for the tetramer and dimer, respectively. $DnaB_C$ formed mixtures of bigger complexes retarded at the top of the gel higher than it would be anticipated by its monomeric state and size (Figure 4). Native DnaB produced undefined diffuse shifts of decreased mobility with dT_{45} indicative of mixed higher order oligomers. These oligomers appeared to be more defined with the larger dT_{90} and dT_{135} oligonucleotides suggesting that they are more stable with longer ssDNA substrates.

To further dissect the interactions with ssDNA we constructed two more truncated polypeptides DnaB(1–365) and DnaB(1–428) (the numbers refer to amino acid residues) (Figure 2C). Both truncated proteins formed stable tetramers and exhibited no signs of significant non-specific aggregation as assessed by sedimentation velocity AUC (Supplementary Figure 4S). DnaB(1–428) formed complexes similar to native DnaB but DnaB(1–365) produced bands that were shifted to a position (marked by an asterisk) much lower than the top of the gel, indicating failure to form higher order oligomers (Figure 4). We conclude that DnaB has two ssDNA binding sites located in $DnaB_N$ and $DnaB_C$. It is likely that binding of DnaB(1–365) to ssDNA is mediated by the site located in $DnaB_N$. Given that $DnaB_C$ is monomeric in solution we also conclude that binding to ssDNA induces oligomerization of this domain. $DnaB_C$ is likely to mediate DNA-induced oligomerization of native DnaB. This oligomerization site is located within residues 365–428 since DnaB(1–365) does not form the big complexes retarded at the top of the gel apparent with native DnaB, $DnaB_C$ and DnaB(1–428). Therefore, if the C-terminal truncation of DnaB observed *in vivo* included residues 365–428 it would abolish the ssDNA-dependent formation of higher order oligomers.

Heparin mimics ssDNA and induces high-order oligomerization of DnaB

To obtain further evidence that DNA binding induces DnaB oligomerization we utilized heparin affinity

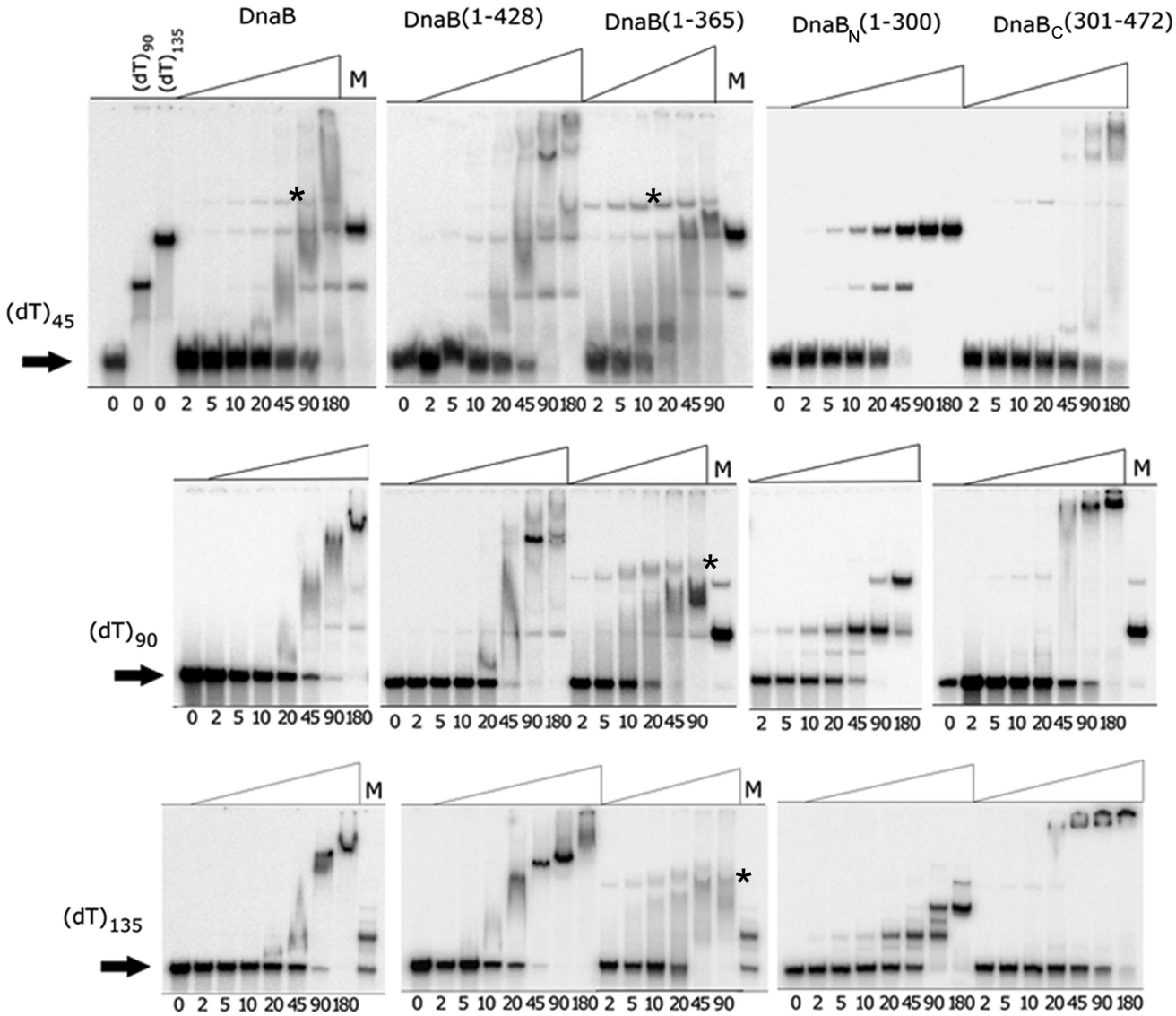

Figure 4. DnaB–ssDNA interactions. Gel shifts showing binding of DnaB polypeptides to ssDNA (dT_{45}, dT_{90} or dT_{135}). The concentrations (μM) of proteins in the binding reactions are shown underneath the lanes of the gels. Lanes M are internal controls showing binding reactions with 45 μM $DnaB_N$. The positions of the slowest migrating bands of DnaB(1–365) are marked by asterisks. The equivalent position with native DnaB is also marked by an asterisk in the dT_{45} gel shift.

chromatography combined with size exclusion chromatography. DnaB, $DnaB_C$ and DnaB(1–428) were loaded to heparin and eluted with an increasing NaCl gradient (Figure 5). DnaB and DnaB(1–428) were eluted as two overlapping peaks (Figure 5A and B). Subsequent analysis of samples from fractions 1–3 by size exclusion chromatography revealed that fraction 1 contained tetramers, whereas fractions 2 and 3 mixtures of higher oligomers (Figure 5A and B). Velocity sedimentation analysis of fractions 1–3 from native DnaB verified the presence of tetramers in fraction 1 with sedimentation coefficient $s^* = 6.8$ and mixtures of higher oligomers in fractions 2 and 3 with a wide distribution of sedimentation coefficients $s^* = 10$–50 (Supplementary Figure 5S). $DnaB_C$ eluted as two separated peaks from the heparin column indicating formation of oligomers. However, subsequent analysis of fractions 1–4 by size exclusion chromatography revealed that they were all monomeric (Figure 5C). The simplest explanation is that $DnaB_C$ oligomers are formed in the presence of DNA but are somewhat unstable in the absence of DNA. Therefore, the presence of $DnaB_N$ may contribute towards greater stability of higher order oligomers in the absence of DNA. DnaB(1–365) did not bind to heparin (data not shown) indicating that the heparin interaction site is between residues 365–428, likely to coincide with the second ssDNA binding site in $DnaB_C$. Since high salt does not induce oligomerization (data not shown) we conclude that binding to heparin mimics binding to DNA and induces the formation of higher order DnaB oligomers. The ssDNA binding and oligomerization sites in $DnaB_C$ are located within residues 365–428.

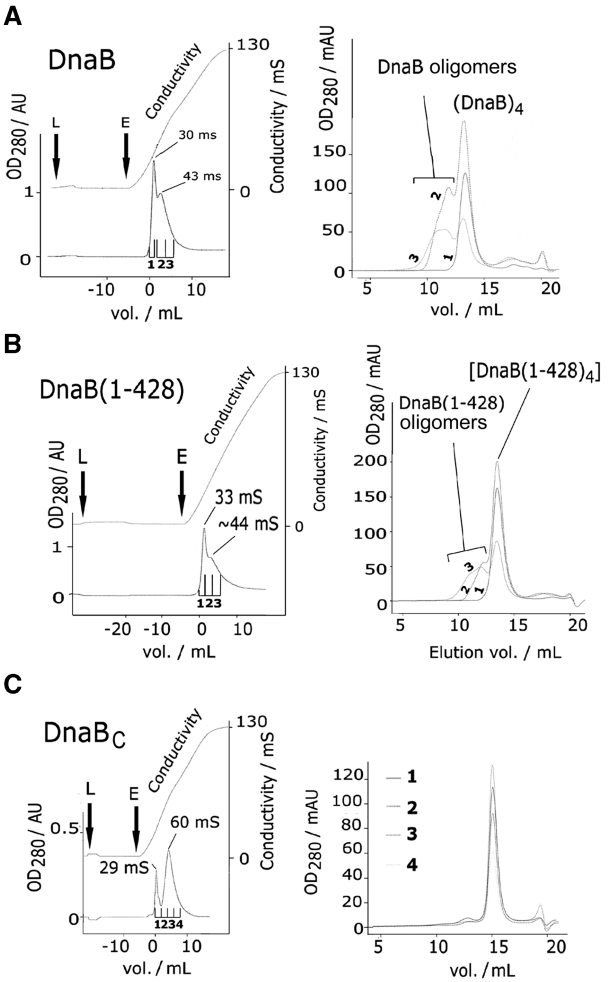

Figure 5. Heparin-induced oligomerization. Chromatograms on the left of panels A–C show elution profiles of DnaB (27 μM), DnaB(1–428) (10 μM) or $DnaB_C$ (30 μM) from a HiTrap Heparin column (GE Healthcare) with a 0–2 M NaCl gradient over 20 ml. Letters L and E mark loading and elution points, respectively. Fractions (2 ml) were collected and numbered 1–3 or 1–4. The conductivity at each peak is indicated. $DnaB_N$ and DnaB(1–365) did not bind to the heparin column under our conditions (data not shown). Gel filtration profiles of the heparin fractions are shown on the right of **A–C**. Samples (0.5 ml) from heparin fractions (1–3) were loaded onto a Superose 6 (HR 10/30, GE Healthcare), except for $DnaB_C$ where Superdex 200 (HR 10/30, GE Healthcare) was used instead. Traces are superimposed and numbered the same as the heparin fractions. Higher order DnaB oligomers are marked accordingly.

DnaB has a dsDNA site within residues 365–428 which also mediates oligomerization

DnaB binds ss and dsDNA (14, 18). Although we showed that DnaB has two ssDNA binding sites within $DnaB_N$ and $DnaB_C$ and forms tetramers and higher order oligomers via $DnaB_N$ and $DnaB_C$ interactions, respectively, it is not clear how it interacts with dsDNA. Using our DnaB fragments and carefully prepared ds dTA_{135} we examined its dsDNA binding properties with gel shift experiments. We discovered that $DnaB_C$ binds dsDNA but $DnaB_N$ does not (Figure 6). Therefore, there is a dsDNA-binding site within $DnaB_C$ whilst $DnaB_N$ binds exclusively ssDNA. $DnaB_C$–dsDNA complexes were of very low electrophoretic mobility. Judging from the

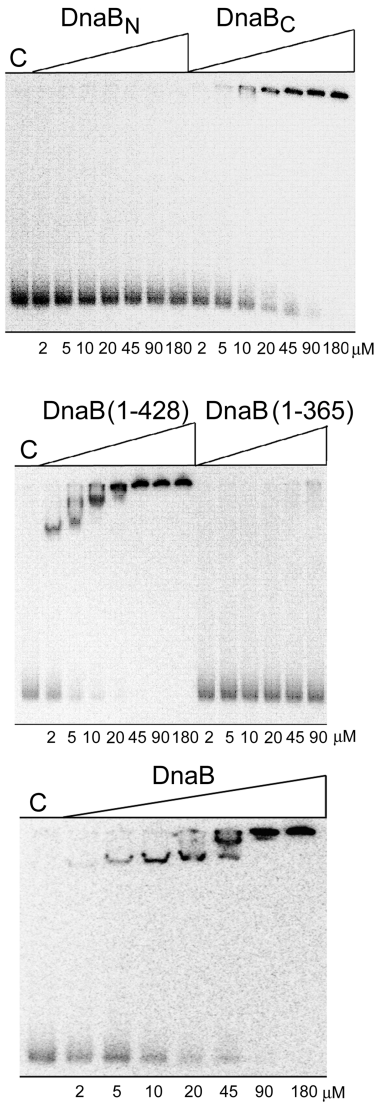

Figure 6. DnaB–dsDNA interactions. Gel shift assays showing binding to dAT_{135} of DnaB polypeptides, as indicated. Lanes C show controls with no proteins.

monomeric state and small size of $DnaB_C$, they are likely to be high-order complexes similar to the ones obtained with ssDNA (Figure 4). To further narrow the location of the dsDNA binding site we examined the DnaB(1–428) and DnaB(1–365) polypeptides (Figure 6). DnaB(1–428) bound to dsDNA forming defined high-order oligomers of very low mobility whereas DnaB(1–365) did not. The dsDNA site is, therefore, located within residues 365–428 coinciding with the area of ssDNA-binding and DNA-induced high-order oligomerization. However, we cannot distinguish whether the ss and dsDNA binding sites in $DnaB_C$ are separate, overlapping or identical.

In vivo truncation is specific for DnaB and confined to soluble not to membrane-associated DnaB

To establish whether the observed proteolysis is a feature of DnaB or generally of other *B. subtilis* primosomal proteins we probed DnaD and DnaI by western blots

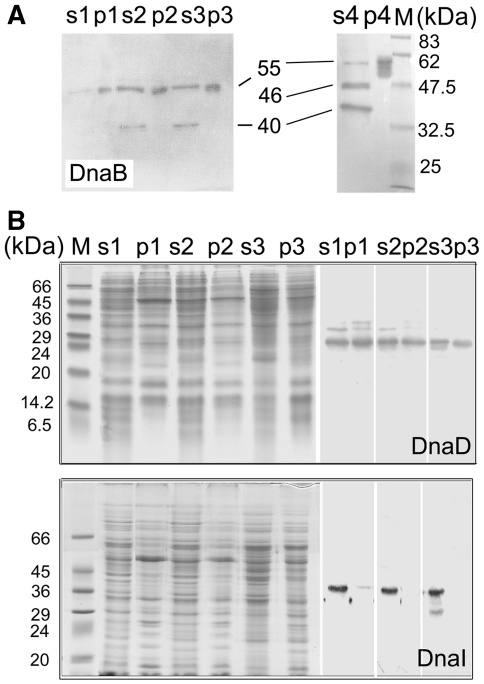

Figure 7. DnaB, DnaD and DnaI levels *in vivo*. (**A**) Western blot of extracts (10 µg) from soluble (s) and pellet (p) fractions at different growth points probed with anti-DnaB. Molecular weight markers are included in lane M. The sizes of DnaB polypeptides are indicated. (**B**) SDS–PAGE (left) and western blot (right) analyses of protein extracts (10 µg) from soluble (s) and pellet (p) fractions at different growth points probed with anti-DnaD and anti-DnaI as indicated. Molecular weight markers are included in lane M. DnaD and DnaI are intact although some non-specific bands just above DnaD and just below DnaI are visible, possibly as a result of insufficient blocking.

(Figure 7). DnaB was present in cytosolic and membrane-associated cell extracts from early, middle and late exponential growth, but truncated versions started to become apparent from middle exponential growth only in cytosolic and not in membrane-associated fractions (Figure 7A). The sizes of fragments did not indicate the formation of distinct domains that added up to the size of native DnaB. Furthermore, the fact that DnaB appears to be intact in the early growth phase and in membrane associated fractions rules out premature termination and/or translation of *dnaB* mRNAs, as there is no reason why such processes should not be apparent in early compared to middle and late growth phases and why only soluble DnaB should be truncated. These data are consistent with our model of C-terminal proteolysis with the separated C-terminal fragment being digested completely. DnaB was mostly truncated in soluble fractions from overnight cultures, compared to membrane-associated fractions where it was somewhat resistant to proteolysis, although some marginal non-specific degradation was also apparent in these samples (Figure 7A). In addition to the 40 kDa fragment, present during exponential growth, another truncated fragment of 46 kDa absent from exponential growth, was apparent in samples from overnight cultures (Figure 7A). DnaD and DnaI were intact (Figure 7B). The former was present in both soluble and membrane-associated fractions and the latter was present only in cytosolic fractions consistent with previous localization studies showing GFP-tagged DnaD and DnaB to be proximal to the membrane and DnaI to be cytosolic (48). We conclude that proteolytic truncation is specific for DnaB and not a general feature of *B. subtilis* DnaD and DnaI primosomal proteins.

Truncated DnaB is depleted from the *oriC*

To investigate the biological significance of this truncation, we carried out comparative ChIP-chip analysis of DnaB–DNA cross linked samples, immunoprecipitated from *B. subtilis* cultures with polyclonal anti-DnaB and anti-$DnaB_C$ antibodies. We argued that if there is extensive C-terminal truncation *in vivo*, then the anti-$DnaB_C$ antibody will immunoprecipitate less DnaB compared to the anti-DnaB antibody, and may allow us to differentiate interaction sites of native and truncated DnaB across the *B. subtilis* genome. We first established that the two antibodies were of comparable strength against native DnaB to allow direct comparison (data not shown). Then *B. subtilis* cultures were grown at $OD_{595} = 0.8$ and treated with formaldehyde. Cross-linked complexes were immunoprecipitated from cell extracts with anti-DnaB and anti-$DnaB_C$ antibodies. Following reversal of cross links, genomic DNA fragments were isolated for microarray analysis. Native and truncated DnaB were found to bind with comparable strength to several sites across the entire genome (Figure 8A and data not shown). Detailed analysis of these genomic sites will be presented elsewhere. Here we have analysed binding to *oriC* and the areas just before and after it (Figure 8B). DnaB was associated with several sites from the middle of *dnaA* to the end of *yaaA* giving several signals with $G/R > 2$ (Figure 8B and C). This region includes one half of the *oriC*, with the other half located upstream of *dnaA* (Figure 8D). By comparison, $DnaB_C$ samples produced much weaker signals ($G/R < 2$) in this region (Figure 8 and Supplementary Figure 6s). For every single one of 23 different oligonucleotide probes exhibiting significant signals ($G/R > 1.5$) in this area, the signals from anti-$DnaB_C$ samples were consistently weaker compared to the equivalent signals from anti-DnaB samples, with differences ranging from 50–300% (Supplementary Figure 6s). By comparison, binding signals elsewhere in the genome were similar in both samples (Figure 8A and data not shown), with comparative sets of different oligonucleotide probes within the same area giving signals of variable strengths between the two samples, i.e. sometimes higher for DnaB samples and sometimes higher for $DnaB_C$ samples (data not shown). This is highly significant as it eliminates random variations between individual oligonucleotide probes within the *oriC* region, indicating that the signal difference observed for all the different 23 sites within this area is a real effect. We conclude that DnaB interacts with *oriC* and that truncated DnaB is depleted at the *oriC* and not in other sites across the genome. Furthermore, the interaction of DnaB with *oriC* is asymmetric, confined to the half *oriC* site downstream of *dnaA*, that includes the AT-rich region, and involves an extended region further downstream encompassing the *dnaN* and *yaaA* genes.

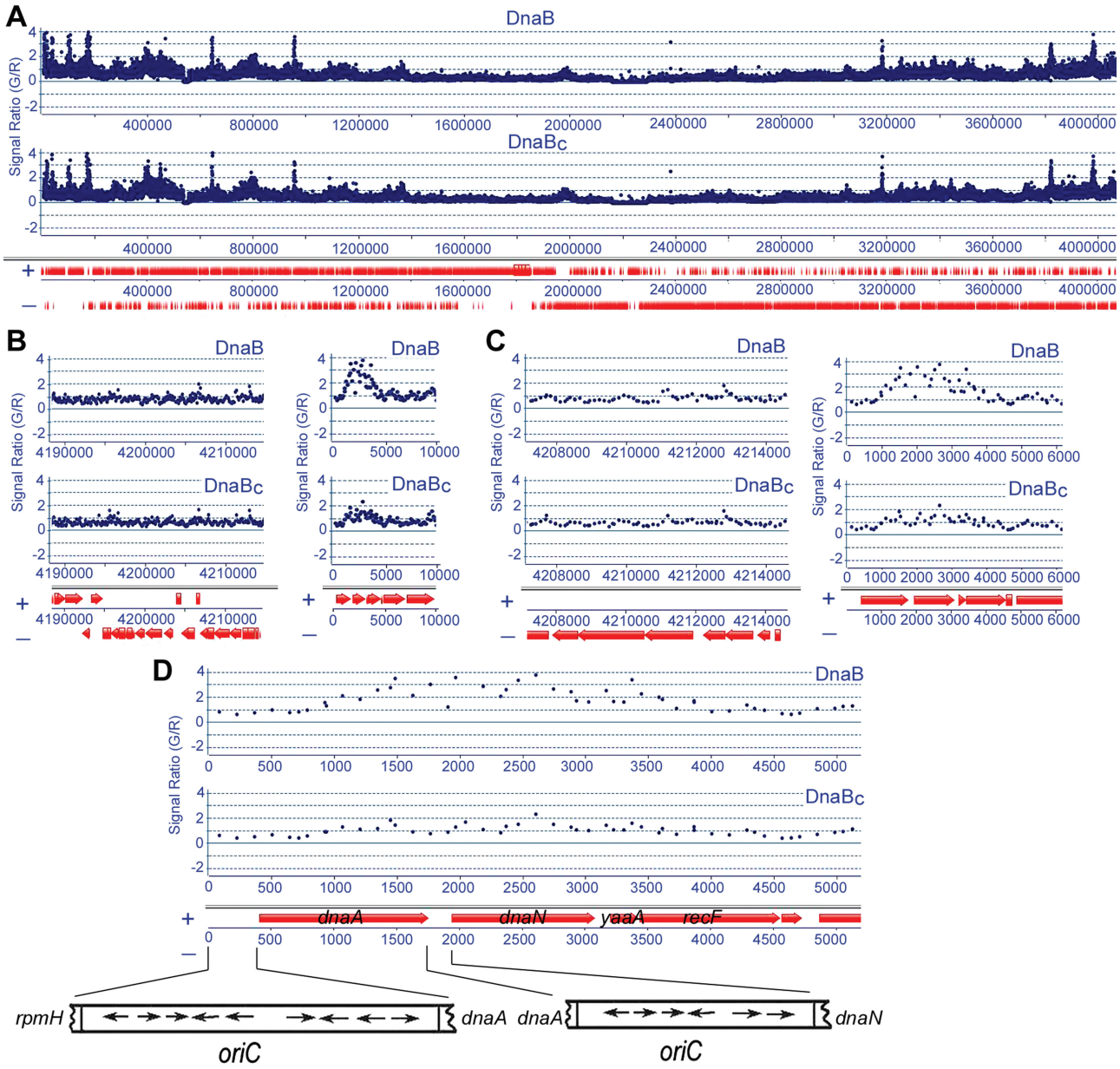

Figure 8. ChIP-chip microarray analysis. (A) Data from ChIP-chip microarray analysis across the entire *B. subtilis* genome using anti-DnaB and anti-$DnaB_C$ polyclonal antibodies, as indicated, showing that the two sets of data are almost identical. The G/R signal ratio of the green and red dyes (the reference sample was in red) and the genomic positions are shown on the y- and x-axes, respectively. The (+) and (−) DNA strands with the entire complement of genes and their positions are shown underneath. (B) Views of the genomic region upstream of the *oriC* (nucleotides 4 190 000–0) and the *oriC* region (nucleotides 0–10 000). Clear association of DnaB with the *oriC* can be seen. The association of $DnaB_C$ with the *oriC* is clearly less compared to DnaB. (C) Expanded views of the genomic region upstream of the *oriC* (nucleotides 4 208 000–0) and the *oriC*-containing region (nucleotides 0–6000), showing clearly reduced association of $DnaB_C$ with *oriC* compared to DnaB. (D) Further expansion of the *oriC*-containing region (0–5000) showing asymmetric association with the *oriC*. Binding of DnaB is apparent from positions 1000–3500. The up- and downstream half sites of the *oriC* on either side of *dnaA* are indicated. DnaA-binding sites are shown by arrows. Comparative signals in this area using the anti-$DnaB_C$ antibody are also shown. Weak association of $DnaB_C$ can also be detected by anti-$DnaB_C$ but the G/R signal ratios are <2 indicating weaker binding compared to DnaB ($G/R > 2$). All 23 individual sites within this region where significant binding is detected (sites with $G/R > 1.5$) the G/R signals from DnaB are significantly higher than those from $DnaB_C$ (Supplementary Figure 6S). We conclude that $DnaB_C$ is depleted from the *oriC*.

DISCUSSION

Biological significance of $DnaB_C$

DnaB is proteolytically truncated in a growth-dependent manner. Truncation is apparent from mid-exponential growth and continues into the stationary phase. It is confined to cytosolic DnaB, membrane-associated DnaB is resistant, and involves the C-terminal region which mediates DNA-induced higher order oligomerization. A partially purified membrane fraction of *B. subtilis* was postulated, as data not shown, to have both native and truncated DnaB, and a cytosolic fraction native

DnaB (26). DnaB was proposed to undergo post-translational modification, involving truncation of a putative hydrophobic N-terminal region (Figure 2C), to become embedded in the cell membrane, although data were never published (26). This, however, is unlikely to be the case as it is the opposite of what we have observed. Our data show that DnaB is intact in early growth and C-terminally truncated in middle-late growth only in cytosolic and not in membrane-associated fractions, although in overnight cultures some non-specific degradation was apparent. It may be that the cytosolic proteases involved have no access to membrane bound DnaB or that the proteolytically sensitive region of DnaB has a different more compact, protease resistant, conformation. The fact that DnaB is intact in early growth and in the membrane associated fraction makes unlikely premature termination and/or translation of *dnaB* mRNA. A careful inspection of the *dnaB* sequence does not reveal any potential termination and/or translational slippage signals.

A shorter DnaB version was reported in the *dnaB19* mutant (carrying the A379T mutation) at permissive temperatures although again no data were ever published (26). The pKW1 plasmid, indigenous to *B. subtilis*, did not replicate in *dnaB19*, whereas it replicated only in dimeric form in *dnaB1* (carrying the P113L mutation within $DnaB_N$), suggesting that $DnaB_C$ may be involved in resolution of newly replicated plasmids (27). Since membrane-associated DnaB is resistant to proteolysis we propose that, in addition to other functions, it may also be involved in plasmid resolution. It is clear that $DnaB_C$ is crucial for initiation of DNA replication and since, as shown here, binds to ss and dsDNA and induces the formation of higher order DnaB oligomers, these activities must be an integral part of its primosomal function.

Linking *oriC* with the cell membrane

The precise structure/function relationships of the DnaB oligomers remain to be elucidated. Here we can only speculate regarding their structure(s). DNA-induced oligomerization and bead-like structures along the DNA have been visualized by AFM (18). In the same studies intense foci suggested that DnaB is capable of forming 'piles' on the DNA with some DnaB molecules inevitably not associated with the DNA in such piles. A speculative suggestion is that this type of oligomerization may be relevant in linking together DnaB associated at the *oriC* with DnaB bound to the membrane. Replication initiation in *B. subtilis* likely occurs at the inner face of the cell membrane (24–26) and DnaB may play a role in controlling this process by recruiting the *oriC* to the inner face of the membrane (29). This may occur by DnaB oligomers forming a cross-bridge with the *oriC* via interactions with DnaD and with the membrane via interactions with membrane bound DnaB. The C-terminal domain may be instrumental in this process with DNA acting as the initial stimulus to cause cooperative cross-tetramer higher order oligomers. Such cross-bridging oligomers may link *oriC* with the inner surface of the cell membrane during exponential growth when DNA replication is most active. As growth slows down the link with the membrane may be broken as DnaB is being truncated.

Helicase loading

Higher order oligomers may, alternatively, represent 'bead-like' structures of successive DnaB-tetramers sandwiched between two DNA molecules similar to the bead-like structures observed by AFM (18). These bead-like structures laterally compact supercoiled DNA (18) but may also be relevant in helicase loading. Somewhat analogous spiral filamentous nucleoprotein structures, that mediate helicase loading, have been suggested for the *E. coli* DnaC helicase loader (49). The actual molecular mechanism of this DNA-induced oligomerization is also not known. We speculate that it may involve an element of co-operativity unleased by binding to DNA and possibly involving conformational changes in $DnaB_C$. Certain mutations in $DnaB_C$ can affect the functional properties of the protein indicating the potential for structural changes in this domain that could affect the function of the protein. For example, *priA* suppressors in *dnaB* have been identified in $DnaB_C$, residues 327, 371 and 404 (10). The mutant DnaB proteins were able to load the replicative DnaC helicase onto ssDNA in a PriA-independent but DnaD- and DnaI-dependent manner. Presumably these mutations within $DnaB_C$ altered the conformation of the protein and hence its ability to load the replicative helicase. In a similar manner DNA-driven conformational changes may induce co-operative DnaB oligomerization via $DnaB_C$.

Regulating access to *oriC*

Truncated DnaB may also be part of a mechanism to regulate access to *oriC* to gradually switch off replication initiation as growth progressively slows down. This can be achieved by abolishing its interaction with DnaD which is believed to be the mechanism by which DnaB is recruited to *oriC* (14, 29). The molecular details of this interaction are not known but, interestingly, the DnaB S371P mutation causes a gain in ssDNA affinity (21) and an increase in its interaction with DnaD (29). S371 is within the 365–418 region predicted by our data to bind DNA and to induce DNA-dependent oligomerization. It is, therefore, probable that $DnaB_C$ mediates the interaction with DnaD. Truncation of DnaB may thus regulate its interaction with DnaD and hence its recruitment to *oriC*.

Self-regulation of native DnaB by interfering with oligomerization

Another possibility is that truncated DnaB may regulate functional oligomerization of native DnaB. Truncated DnaB, with an intact $DnaB_N$, will still be able to form mixed tetramers with native DnaB thus interfering with its action. An example of interference with

oligomerization by a truncated version of the same protein as a means of regulating its function, can be seen in the case of H-NS. *E. coli* H-NS is a nucleoid associated protein and a global transcriptional regulator (mainly repressor) of several genes. It has a bipartite structure with a coiled-coil N-terminal domain involved in oligomerization and a DNA-binding C-terminal domain (50). Expression of the N-terminal domain has a dominant inhibitory effect on native H-NS mediated repression by interfering with its oligomerization via their mutual coiled-coil domains (51, 52). Furthermore, a naturally-occurring family of H-NS truncated (H-NST) proteins from enteropathogenic *E. coli* (EPEC), that lack the DNA-binding domain, can functionally antagonize H-NS mediated repression by interfering with oligomerization (53). It is also possible that truncated DnaB may be required for additional unidentified functions mediated exclusively via $DnaB_N$.

DnaB has multiple DNA-binding sites

DnaB has two ssDNA-binding sites located in $DnaB_N$ and $DnaB_C$ and a dsDNA-binding site within residues 365–428. This region exhibits similarity to a region of the putative replication initiation phage protein Gp49 (29). The S371P point mutation results in a 50-fold increased affinity for ssDNA (21). However, it is unlikely that a serine residue would be involved in a direct interaction with DNA. Instead, it is likely that a proline in this position has affected local secondary structure making it more favourable to bind ssDNA. At this stage, it is not clear whether the ss and dsDNA-binding sites in $DnaB_C$ are separate, overlapping or identical. An antibody against a peptide encompassing residues 444–458 inhibits binding to the pUB110 plasmid (47). This is outside the 365–428 region but the observed DNA binding defect is likely to be due to steric problems when a bulky antibody is bound in the vicinity. Further mutagenesis studies will be required to clarify this.

Asymmetric association of DnaB with *oriC*

DnaB is a non-specific DNA binding protein recruited to the *oriC* via a protein–protein interaction with DnaD which in turn is recruited by an interaction with DnaA. Chromatin immunoprecipitation targets DnaB that has been recruited at *oriC* by the DnaA–DnaD complex. Our ChIP-chip data suggest that truncated DnaB is depleted at *oriC* and that the association of DnaB with *oriC* is asymmetric and involves the half site located downstream of *dnaA*. This is the site that contains the AT-rich sequence thought to melt prior to helicase-loading (54). It makes sense for DnaB to be present in the vicinity of this site if it is to participate directly in loading of the DnaC helicase. There is no association of DnaB with the half *oriC* site located upstream of *dnaA*. Instead, DnaB binds to an extended area from the middle of *dnaA* to the end *of yaaA* suggesting that remodelling of the *oriC* during initiation of DNA replication is extensive and involves a wide-area beyond the core *oriC* sites. Loading of the replicative *E. coli* DnaB helicase at *oriC* has also been suggested to involve asymmetric binding of the helicase loader DnaC which through a direct interaction with ATP-charged DnaA recruits a helicase hexamer to one DNA strand, while the second helicase hexamer is recruited to the opposite strand by DnaA alone (49). *E. coli* DnaC has been postulated to form right-handed spiral oligomers that are likely to reflect the formation of true filaments on the DNA during helicase loading (49). DnaI, the *B. subtilis* homologue of *E. coli* DnaC, has an equivalent ATPase C-terminal domain (33, 55) while its co-loader DnaB can also form bead-like structures on DNA (18). It would be interesting to determine whether the asymmetric association of DnaB with *oriC* reflects loading of the replicative helicase DnaC by the DnaI–DnaB dual loader to one of the DNA strands, equivalent to the DnaC-mediated helicase loading in *E. coli*.

SUPPLEMENTARY DATA

Supplementary Data are available at NAR Online.

ACKNOWLEDGEMENTS

We thank Charikleia Ioannou for help with preliminary western blots and Ed Bolt for help with oligonucleotide purifications.

FUNDING

Biotechnology and Biological Sciences Research Council (BBSRC) grant to PS (BB/E006450/1). Funding for open access charge: Biotechnology and Biological Sciences Research Council (BBSRC).

Conflict of interest statement. None declared.

REFERENCES

1. Mott,M.L. and Berger,M. (2007) DNA replication initiation: mechanisms and regulation in bacteria. *Nat. Rev. Microbiol.*, **5**, 343–354.
2. Messer,W. (2002) The bacterial replication initiator DnaA. DnaA and *oriC*, the bacterial mode to initiate DNA replication. *FEMS Microbiol. Rev.*, **26**, 355–374.
3. Mackiewicz,P., Zakrewsjak-Crewinska,J., Zawilak,A., Dudek,M.R. and Cebrat,S. (2004) Where does bacterial replication start? Rules for predicting the *oriC* region. *Nucleic Acids Res.*, **32**, 3781–3791.
4. Erzberger,J.P., Pirruccello,M.M. and Berger,J.M. (2002) The structure of bacterial DnaA: implications for general mechanisms underlying DNA replication initiation. *EMBO J.*, **21**, 4763–4773.
5. Cunningham,E.L. and Berger,J.M. (2005) Unraveling the early steps of prokaryotic replication. *Curr. Opinion Struct. Biol.*, **15**, 68–76.
6. Kaguni,J.M. (2006) DnaA: controlling the initiation of bacterial DNA replication and more. *Annu. Rev. Microbiol.*, **60**, 351–371.
7. Heller,R.C. and Marians,K.J. (2006) Replisome assembly and the direct restart of stalled replication forks. *Nat. Rev. Mol. Cell Biol.*, **7**, 932–943.
8. Heller,R.C. and Marians,K.J. (2005) The disposition of nascent strands at stalled replication forks dictates the pathway of replisome loading during restart. *Mol. Cell*, **17**, 733–743.

9. Bruand,C., Ehrlich,S.D. and Janniere,L. (1995) Primosome assembly site in *Bacillus subtilis*. *EMBO J.*, **14**, 2642–2650.
10. Bruand,C., Farache,M., McGovern,S., Ehrlich,S.D. and Polard,P. (2001) DnaB, DnaD and DnaI proteins are components of the *Bacillus subtilis* replication restart primosome. *Mol. Microbiol.*, **42**, 245–255.
11. Li,Y., Kurokawa,K., Matsuo,M., Fukuhara,N., Murakami,K. and Sekimizu,K. (2004) Identification of temperature-sensitive *dnaD* mutants of *Staphylococcus aureus* that are defective in chromosome DNA replication. *Mol. Genet. Genomics*, **271**, 447–457.
12. Li,Y., Kurokawa,K., Reutimann,L., Mizumura,H., Matsuo,M. and Sekimizu,K. (2007) DnaB and DnaI temperature-sensitive mutants of *Staphylococcus aureus*: evidence for involvement of DnaB and DnaI in synchrony regulation of chromosome replication. *Microbiology*, **153**, 3370–3379.
13. Ishigo-Oka,D., Ogasawara,N. and Moriya,S. (2001) DnaD protein of *Bacillus subtilis* interacts with DnaA, the initiator protein of replication. *J. Bacteriol.*, **183**, 2148–2150.
14. Marsin,S., McGovern,S., Ehrlich,S.D., Bruand,C. and Polard,P. (2001) Early steps of *Bacillus subtilis* primosome assembly. *J. Biol. Chem.*, **276**, 45818–45825.
15. Turner,I.J., Scott,D.J., Allen,S., Roberts,C.J. and Soultanas,P. (2004) The *Bacillus subtilis* DnaD protein: a putative link between DNA remodeling and initiation of DNA replication. *FEBS Lett.*, **577**, 460–464.
16. Zhang,W., Allen,S., Roberts,C.J. and Soultanas,P. (2006) The *Bacillus subtilis* primosomal protein DnaD untwists supercoiled DNA. *J. Bacteriol.*, **188**, 5487–5493.
17. Zhang,W., Machón,C., Orta,A., Phillips,N., Roberts,C.J., Allen,S. and Soultanas,P. (2008) Single-molecule atomic force spectroscopy reveals that DnaD forms scaffolds and enhances duplex melting. *J. Mol. Biol.*, **377**, 706–714.
18. Zhang,W., Carneiro,M.J.V.M., Turner,I.J., Allen,S., Roberts,C.J. and Soultanas,P. (2005) The *Bacillus subtilis* DnaD and DnaB proteins exhibit different DNA remodeling activities. *J. Mol. Biol.*, **351**, 66–75.
19. Carneiro,M.J.V.M., Zhang,W., Ioannou,C., Scott,D.J., Allen,S., Roberts,C.J. and Soultanas,P. (2006) The DNA-remodelling activity of DnaD is the sum of oligomerisation and DNA-binding activities on separate domains. *Mol. Microbiol.*, **60**, 917–924.
20. Schneider,S., Zhang,W., Soultanas,P. and Paoli,M. (2008) Structure of the N-terminal oligomerisation domain of DnaD reveals a unique tetramerization motif and provides insights into scaffold formation. *J. Mol. Biol.*, **376**, 1237–1250.
21. Bruand,C., Velten,M., McGovern,S., Marsin,S., Serena,C., Ehrlich,S.D. and Polard,P. (2005) Functional interplay between the *Bacillus subtilis* DnaD and DnaB proteins essential for initiation and re-initiation of DNA replication. *Mol. Microbiol.*, **55**, 1138–1150.
22. Velten,M., McGovern,S., Marsin,S., Ehrlich,S.D., Noirot,P. and Polard,P. (2003) A two-protein strategy for the functional loading of a cellular replicative DNA helicase. *Mol. Cell*, **11**, 1009–1020.
23. Nunez-Ramirez,R., Velten,M., Rivas,G., Polard,P., Carazo,J.M. and Donate,L.E. (2007) Loading a ring: Structure of the *Bacillus subtilis* DnaB protein, a co-loader of the replicative helicase. *J. Mol. Biol.*, **367**, 764–769.
24. Winston,S. and Sueoka,N. (1980) DNA-membrane association is necessary for initiation of chromosomal and plasmid replication in *Bacillus subtilis*. *Proc. Natl Acad. Sci. USA*, **77**, 2834–2838.
25. Hoshino,T., McKenzie,T., Schmidt,S., Tanaka,T. and Sueoka,N. (1987) Nucleotide sequence of *Bacillus subtilis dnaB*: a gene essential for DNA replication initiation and membrane attachment. *Proc. Natl Acad. Sci. USA*, **84**, 653–657.
26. Sueoka,N. (1998) Cell membrane and chromosome replication in *Bacillus subtilis*. *Prog. Nucleic Acids Res.*, **59**, 34–53.
27. Watabe,K. and Forough,R. (1987) Effects of temperature sensitive variants of the *Bacillus subtilis dnaB* gene on the replication of low-copy-number plasmid. *J. Bacteriol.*, **169**, 4141–4146.
28. Sato,Y., McCollum,M., McKenzie,T., Laffan,J., Zuberi,A. and Sueoka,N. (1991) *In vitro* type II binding of chromosomal DNA to membrane in *Bacillus subtilis*. *J. Bacteriol.*, **173**, 7732–7735.
29. Rokop,M.E., Auchtung,J.M. and Grossman,A.D. (2004) Control of DNA replication initiation by recruitment of an essential initiation protein to the membrane of *Bacillus subtilis*. *Mol. Microbiol.*, **52**, 1757–1767.
30. Livak,K.J. and Schmittgen,T.D. (2001) Analysis of relative gene expression data using real-time quantitative PCR and the $2^{-\Delta\Delta C_T}$ method. *Methods*, **25**, 402–408.
31. Bradford,M. (1976) A rapid and sensitive method for the quantitation of microgram quantities of protein utilizing the principle of protein-dye binding. *Anal. Biochem.*, **72**, 248–254.
32. Adams,J.C. (1977) Technical considerations on the use of horseradish peroxidase as a neuronal marker. *Neuroscience*, **2**, 141–145.
33. Soultanas,P. (2002) A functional interaction between the putative primosomal protein DnaI and the main replicative DNA helicase DnaB in Bacillus. *Nucleic Acids Res.*, **30**, 966–974.
34. Schuck,P. (2000) Size-distribution analysis of macromolecules by sedimentation velocity ultracentrifugation and Lamm equation modeling. *Biophys J.*, **78**, 1606–1619.
35. Schuck,P. (1998) Sedimentation analysis of noninteracting and self-associating solutes using numerical solutions to the Lamm equation. *Biophys J.*, **75**, 1503–1512.
36. Schuck,P. (2003) On the analysis of protein self-association by sedimentation velocity analytical ultracentrifugation. *Anal Biochem.*, **320**, 104–124.
37. Cho,B.K., Knight,E.M., Barrett,C.L. and Palsson,B.Ø. (2008) Genome-wide analysis of Fis binding in *Escherichia coli* indicates a causative role for A-/AT-tracts. *Genome Res.*, **18**, 900–910.
38. Herrick,J., Kohiyama,M., Atlung,T. and Hansen,F.G. (1996) The initiation mess? *Mol. Microbiol.*, **19**, 659–666.
39. Ogura,Y., Imai,Y., Ogasawara,N. and Moriya,S. (2001) Autoregulation of the *dnaA-dnaN* operon and effects of DnaA protein levels on replication initiation in *Bacillus subtilis*. *J. Bacteriol.*, **183**, 3833–3841.
40. de Vries,Y.P., Hornstra,L.M., de Vos,W.M. and Abee,T. (2004) Growth and sporulation of *Bacillus cereus* ATCC 14579 under defined conditions: temporal expression of genes for key sigma factors. *Appl. Environ. Microbiol.*, **70**, 2514–2519.
41. Bruand,C. and Ehrlich,S.D. (1995) The *Bacillus subtilis dnaI* gene is part of the *dnaB* operon. *Microbiol*, **141**, 1199–1200.
42. Cole,C., Barber,J.D. and Barton,G.J. (2008) The Jpred 3 secondaray structure prediction server. *Nucleic Acids Res.*, **36(Web Server issue)**, W197–W201.
43. Larkin,M.A., Blackshields,G., Brown,N.P., Chenna,R., McGettigan,P.A., McWilliam,H., Valentin,F., Wallacxe,I.M., Wim,A., Lopez,R. *et al.* (2007) Clustal W and Clustal X version 2.0. *Bioinformatics*, **23**, 2947–2948.
44. Henikoff,S. and Henikoff,J.G. (1992) Amino acid substitution matrices from protein blocks. *Proc. Natl Acad. Sci. USA*, **89**, 10915–10919.
45. Ogasawara,N., Moriya,S. and Mazza,P.G. (1986) Nucleotide sequence and organization of *dnaB* gene and neighbouring geneson the *Bacillus subtilis* chromosome. *Nucleic Acids Res.*, **14**, 9989–9999.
46. Kracilek,A.V., Day,A.J., Wake,R.G. and King,G.F. (1991) A sequence similarity between proteins involved in initiation and termination of bacterial chromosome replication. *Biochem J.*, **275(Pt 3)**, 823.
47. Watabe,K. and Forough,R. (1987) Identification of the product of *dnaB* gene in *Bacillus subtilis*. *Biochem. Biophys. Res. Commun.*, **145**, 861–867.
48. Meile,J.C., Wu,L.J., Ehrlich,S.D., Errington,J. and Noirot,P. (2006) Systematic localization of proteins fused to the green fluorescent protein in *Bacillus subtilis*: identification of new proteins at the DNA replication factory. *Proteomics*, **6**, 2135–2146.
49. Mott,M.L., Erzberger,J.P., Coons,M.M. and Berger,J. (2008) Structural synergy and molecular crosstalk between bacterial helicase loaders and replication initiators. *Cell*, **135**, 623–634.
50. Dorman,C.J., Hinton,J.C.D. and Free,A. (1999) Domain organization and oligomerisation among H-NS-like nucleoid-associated proteins in bacteria. *Trends Microbiol.*, **7**, 124–128.
51. Williams,R.M., Rimsky,S. and Buc,H. (1996) Probing the structure function and interactions of the *Escherichia coli* H-NS

and StpA proteins by using dominant negative derivatives. *J. Bacteriol.*, **178**, 4335–4343.
52. Free,A., Porter,M.E., Deighan,P. and Dorman,C.J. (2001) Requirement for the molecular adapter function of StpA at the *Escherichia coli bgl* promoter depends upon the level of truncated H-NS protein. *Mol. Microbiol.*, **42**, 903–918.
53. Williamson,H.S. and Free,A. (2005) A truncated H-NS-like protein from enteropathogenic *Escherichia coli* acts as an H-NS antagonist. *Mol. Microbiol.*, **55**, 808–827.
54. Krause,M., Ruckert,B., Lurz,R. and Messer,W. (1997) Complexes at the replication origin of *Bacillus subtilis* with homologous and heterologous DnaA protein. *J. Mol. Biol.*, **274**, 365–380.
55. Ioannou,C., Schaeffer,P.M., Dixon,N.E. and Soultanas,P. (2006) Helicase binding to DnaI exposes a cryptic DNA-binding site during helicase loading in *Bacillus subtilis*. *Nucleic Acids Res.*, **34**, 5247–5258.